Hypernuclear matter in a complete SU(3) symmetry group

Luiz L. Lopes,* and Debora P. Menezes
Departamento de Fisica, CFM, Universidade Federal de Santa Catarina; C.P. 476, CEP 88.040-900, Florianópolis, SC, Brazil
(Received 22 October 2013; revised manuscript received 14 January 2014; published 19 February 2014)

Using the well-known quantum hadrodynamics, we study the effects of meson-hyperon coupling constants on the onset of hyperons in dense nuclear matter. We use the SU(3) symmetry group to fix all these coupling constants, constrained to experimental nuclear matter results and astrophysical observations. While the discovery of massive pulsars PSR J1614-2230 and PSR J0348+0432 points towards a very stiff equation of state at very large densities, results from heavy-ion collisions point in the opposite direction for densities below 5 times the nuclear saturation density. We study some well-known parametrizations and see that most of them cannot satisfy both types of constraints. Indeed, although in our model we can simulate a 2.25 $M_\odot$ hyperonic neutron star, the heavy-ion collision constraints limit the maximum mass around 2.06 $M_\odot$.

DOI: 10.1103/PhysRevC.89.025805 PACS number(s): 24.10.Jv, 21.60.Fw, 26.60.Kp, 14.20.Jn

I. INTRODUCTION

The physics of nuclear matter is well understood around the nuclear saturation density, and most physical parameters are known within very little uncertainties. However, the physics of very high densities is far from being fully understood. The discovery of massive pulsars PSR J1614-2230 [1] and PSR J0348+0432 [2] indicates a very stiff equation of state (EOS) for densities above the saturation point. At such high densities, particles with some strange content can be created, since they are energetically favorable once the the Fermi energy of the nucleons becomes of the order of their rest masses. The onset of hyperons softens the EOS and reduces the possible maximum mass of the correspondent neutron star [3], which may cause a conflict between the astrophysical observations and the theoretical previsions.

Generally, models containing hyperons predict neutron stars with masses below 1.9 $M_\odot$, which would exclude the possibility of hyperons in their cores. Using Brueckner-Hartree-Fock (BHF) models, previous studies found maximum masses between 1.26 $M_\odot$ and 1.47 $M_\odot$ [4–7]. Other nonrelativistic phenomenological models increase (but not enough) the maximum mass to 1.8 $M_\odot$ [8]. Another possibility is to use relativistic quantum hadrodynamic (QHD) models [9], where the strong interaction is simulated by the exchange of massive mesons through Yukawa potentials. While most hypernuclear EOS predict neutron star masses below 2 $M_\odot$, even in QHD [3,10–13], a few parametrizations succeed in describing very massive hyperonic neutron stars [14–16]. Strange mesons as extra mediators of the hyperon-hyperon interactions were first introduced in Refs. [17,18] and a clever mechanism to increase the maximum mass of neutron stars with hyperons in their core (hyperonic stars) is to include an additional strange vector meson [19,20]. This approach has the advantage of not affecting any of the well-known nuclear properties, just pushing away the hyperon threshold and suppressing their fraction at high densities.

The major difficulty when hyperons are present is to fix the coupling constants of these particles with the mesons. It is very common in the literature to use the hybrid SU(6) symmetry group [21] to fix the coupling of the hyperons with the vector mesons, while the coupling with the scalar ones is fixed through the hyperon potential depth. Despite the insight gained by the knowledge of the hyperon potential depth, the problem is far from solved. While the Λ potential depth (U_Λ) is known to be equal to -28 MeV [22,23], the Σ and Ξ potentials (U_Σ, U_Ξ) present a huge uncertainty and not even the signs of these potentials are well defined [23,24], although there are canonical values normally used in modern literature ($U_\Sigma = +30$ MeV and $U_\Xi = -18$ MeV) [25].

The use of the SU(6) parametrization for the vector mesons along the canonical hyperon potential depths create new problems: The maximum masses usually achieved are lower than 2.0 $M_\odot$ [16,19], in disagreement with recent observations. An attempt to conciliate massive neutron stars with the SU(6) theory was performed in two works [19,26], where the authors varied the hyperon potentials in an *ad hoc* way. They found that the hyperon potential has but little influence on the maximum mass. Another *ad hoc* approach was proposed by Glendenning *et al.* [22], where the meson hyperon coupling was fixed to reproduce the U_Λ potential [27], considering that all the hyperons couple in the same way. With this approach, a family of hyperon meson parametrization was obtained. Although it can describe massive neutron stars the results are strongly model dependent, and the maximum mass can vary 100%, from 1.2 to 2.4 solar masses [3]. Nevertheless, this approach is widely used in the literature [3,12,14,16,28], and we call it the *Glendenning conjecture* (GC).

Other proposals consider the inclusion of a new vector meson to mediate hyperon-hyperon interaction without affecting nuclear matter [19,20] and the break of SU(6) symmetry of the isoscalar-vector meson to a more general SU(3) flavor symmetry group [20,29]. The use of SU(3) instead of the SU(6) symmetry produces very massive hyperonic neutron stars, with maximum masses as high as 2.3 $M_\odot$ [20]. The main problem related to the previous SU(3) symmetry-based models is that while the isoscalar-vector mesons are allowed to break the SU(6) symmetry, the isovector-vector meson is forced to obey it, which sounds rather artificial. The scalar meson coupling is poorly obtained, since it is fixed from a pure

*luiz_kiske@yahoo.com.br

phenomenological basis. Moreover, results of the past decade in heavy-ion collisions (HICs) have shown that although the EOS has to be very stiff at large densities, it should be soft for densities below 5 times the nuclear saturation point [30,31], in disagreement with the EOS that produces high-mass neutron stars.

In this work, we study a QHD-based model with three parametrizations: GM1, GM3 [22], and NL3 [32] in the traditional $\sigma\omega\rho$ and in the more exotic $\sigma\omega\rho\phi$ models [19,20]. We propose new parametrization families in such a way that all hyperon meson couplings are in accordance with the SU(3) symmetry group instead of only the isoscalar-vector ones. We do that tying the parameters of the scalar meson group with the vector ones, in such a way to describe the well-known $U_\Lambda = -28$ MeV, and let the uncertain U_Σ and U_Ξ be determined only by the symmetry group properties, without any other phenomenological input. We also use one of the GC parametrization in the standard $\sigma\omega\rho$ model to compare the differences arising from a full symmetric model with respect to a full phenomenological one. Then we calculate some physical quantities as particle fractions, strangeness fraction, and speed of sound in the hypernuclear medium, since they may be important to investigate quark-hadron phase transitions [33]. In order to validate our proposal we compare our results with those obtained from HIC and astrophysical observations.

This paper is organized as follows: in Sec. II we discuss the QHD formalism and calculate the EOS and the meson-field equations. In Sec. III we display our choice of parametrizations and some of the physical quantities they foresee for nuclear matter. We also display all the hyperon meson coupling constants obtained from the SU(3) symmetry and the GC approach and the related previsions for the hyperon potential depths. In Sec. IV we show the results of several parametrization sets and discuss some observational, experimental, and theoretical constraints. The conclusions are presented in Sec. V and the calculations of the hyperon-meson coupling constants within a complete SU(3) symmetry are developed in the Appendix.

II. FORMALISM

We use an extended version of the relativistic QHD [9], whose Lagrangian density reads as follows:

$$\mathcal{L}_{\rm QHD} = \sum_B \bar{\psi}_B \left[\gamma^\mu \left(i\partial_\mu - g_{BB\omega}\omega_\mu - g_{BB\phi}\phi_\mu - g_{BB\rho}\frac{1}{2}\vec{\tau}\cdot\vec{\rho}_\mu \right) - (m_B - g_{BB\sigma}\sigma) \right] \psi_B - U(\sigma) + \frac{1}{2}\left(\partial_\mu\sigma\,\partial^\mu\sigma - m_s^2\sigma^2\right) + \frac{1}{4}\Omega^{\mu\nu}\Omega_{\mu\nu} + \frac{1}{2}m_v^2\omega_\mu\omega^\mu - \frac{1}{4}\Phi^{\mu\nu}\Phi_{\mu\nu} + \frac{1}{2}m_\phi^2\phi_\mu\phi^\mu + \frac{1}{2}m_\rho^2\vec{\rho}_\mu\cdot\vec{\rho}^{\,\mu} - \frac{1}{4}\mathbf{P}^{\mu\nu}\cdot\mathbf{P}_{\mu\nu}, \tag{1}$$

where the sum in B stands just for the nucleons or for all the baryon octet, depending on our choice for the star consitituents; ψ_B are the baryonic Dirac fields; and σ, ω_μ, ϕ_μ, and $\vec{\rho}_\mu$ are the mesonic fields. The g's are the Yukawa coupling constants that simulate the strong interaction; m_B is the mass of the baryon B; and m_s, m_v, m_ϕ, and m_ρ are the masses of the σ, ω, ϕ, and ρ mesons, respectively. The antisymmetric mesonic field strength tensors are given by their usual expressions as presented in Ref. [3]. The $U(\sigma)$ is the self-interaction term introduced in Ref. [34] to reproduce some of the saturation properties of the nuclear matter and is given by the following:

$$U(\sigma) = \frac{1}{3!}\kappa\sigma^3 + \frac{1}{4!}\lambda\sigma^4. \tag{2}$$

Finally, $\vec{\tau}$ are the Pauli matrices. In order to describe a neutral, chemically stable hypernuclear matter, we add leptons as free Fermi gases as follows:

$$\mathcal{L}_{\rm lep} = \sum_l \bar{\psi}_l[i\gamma^\mu\partial_\mu - m_l]\psi_l, \tag{3}$$

where the sum runs over the two lightest leptons (e and μ).

The nucleon masses are assumed to be $N = 939$ MeV, the Σ triplet masses are 1193 MeV, the Λ^0 mass is 1116 MeV, and the Ξ doublet masses are 1318 MeV. The electron and muon masses are 0.511 and 105.6 MeV, respectively. The vector meson masses are 783 MeV for the ω and 1020 MeV for the ϕ. With GM1 and GM3 parametrizations, we have 770 MeV for the ρ, while with the NL3, the ρ mass is 763 MeV. All these masses are the physical ones, corresponding to values close to those found experimentally. The scalar meson σ may be regarded as the $\epsilon(760)$ [35–37] with a fictitious mass of 512 MeV for GM1 and GM3, and 508 MeV for NL3, to agree with the parametrizations proposed in Refs. [22,32].

To solve the equations of motion, we use the mean-field approximation (MFA), where the meson fields are replaced by their expectation values, i.e, $\sigma \to \langle\sigma\rangle = \sigma_0$, $\omega^\mu \to \delta_{0\mu}\langle\omega^\mu\rangle = \omega_0$ and $\rho^\mu \to \delta_{0\mu}\langle\rho^\mu\rangle = \rho_0$. The MFA gives us the following eigenvalue for the baryon energy [3]:

$$E_B = \sqrt{k^2 + M_B^{*2}} + g_{BB\omega}\omega_0 + g_{BB\rho}\frac{\tau_3}{2}\rho_0, \tag{4}$$

where M_B^* is the baryon effective mass, $M_B^* \doteq m_B - g_{BB\sigma}\sigma_0$.

For the leptons, the energy eigenvalues are those of the free Fermi gas,

$$E_l = \sqrt{k^2 + m_l^2}, \tag{5}$$

and the meson fields become

$$\omega_0 = \sum_B \frac{g_{BB\omega}}{m_v^2} n_B, \tag{6}$$

$$\phi_0 = \sum_B \frac{g_{BB\phi}}{m_\phi^2} n_B, \tag{7}$$

$$\rho_0 = \sum_B \frac{g_{BB\rho}}{m_\rho^2}\frac{\tau_3}{2} n_B, \tag{8}$$

$$\sigma_0 = \sum_B \frac{g_{BB\sigma}}{m_s^2} n_{SB} - \frac{1}{2}\frac{\kappa}{m_s^2}\sigma_0^2 - \frac{1}{6}\frac{\lambda}{m_s^2}\sigma_0^3, \tag{9}$$

where n_{SB} is the scalar density and n_B is the number density of the baryon B,

$$n_{SB} = \int_0^{k_{fB}} \frac{M^*}{\sqrt{k^2 + M^{*2}}} \frac{k^2}{\pi^2} dk,$$
$$n_B = \frac{k_{fB}^3}{3\pi^2}, \quad \text{and} \quad n = \sum_B n_B. \tag{10}$$

To describe the properties of the hypernuclear matter, we calculate the EOS from statistical mechanics [38]. The baryons and leptons, being fermions, obey the Fermi-Dirac distribution. In order to compare our results with experimental and observational constraints, we next study nuclear and stellar systems at zero temperature. In this case the Fermi-Dirac distribution becomes the Heaviside step function. The energy densities of baryons, leptons, and mesons (which are bosons) read as follows:

$$\epsilon_B = \frac{1}{\pi^2} \sum_B \int_0^{k_f} \sqrt{k^2 + M_B^{*2}} k^2 dk, \tag{11}$$

$$\epsilon_l = \frac{1}{\pi^2} \sum_l \int_0^{k_f} \sqrt{k^2 + m_l^2} k^2 dk, \tag{12}$$

$$\epsilon_m = \frac{1}{2}\left(m_s^2\sigma_0^2 + m_v^2\omega_0^2 + m_\phi^2\phi_0^2 + m_\rho^2\rho_0^2\right) + U(\sigma), \tag{13}$$

where k_f is the Fermi momentum, and we have already used the fact that the fermions have degeneracy equal to 2. The total energy density is the sum of the partial ones,

$$\epsilon = \epsilon_B + \epsilon_l + \epsilon_m, \tag{14}$$

and the pressure is calculated via thermodynamic relations,

$$P = \sum_f \mu_f n_f - \epsilon, \tag{15}$$

where the sum runs over all the fermions ($f = B,l$) and μ is the chemical potential, which corresponds exactly to the energy eigenvalue at $T = 0$.

III. MODEL PARAMETERS

We use three standard QHD parametrizations: GM1, GM3 [14,22], and NL3 [32] to describe five input parameters as follows: nuclear saturation density, n_0; binding energy per baryon, B/A; effective nucleon mass, M^*; nuclear compression modulus, K; and the symmetry energy coefficient S_0 and its slope L. Table I resumes the parametrizations and the bulk nuclear matter values they generate.

The ϕ meson, which carries strangeness, is generally disregarded. The models where it is not present are the traditional $\sigma\omega\rho$ models. When the ϕ is present, we have chosen to call the models as $\sigma\omega\rho\phi$ models [17–20,39,40].

In order to fix the hyperon meson couplings, we use two different approaches. The first one relies on a pure phenomenological basis and we call it GC. Within the GC parametrization, the ϕ meson is never present. It assumes

TABLE I. Parameters and physical quantities for GM1, GM3, and NL3 models.

	GM1	GM3	NL3
$g_{NN\sigma}$	8.910	8.175	10.217
$g_{NN\omega}$	10.610	8.712	12.868
$g_{NN\phi}$	0.0	0.0	0.0
$g_{NN\rho}$	8.196	8.259	8.948
κ/M_N	0.005894	0.017318	0.0041014
λ	−0.006426	−0.014526	−0.015921
n_0 (fm^{-3})	0.153	0.153	0.148
M^*/M	0.70	0.78	0.60
K (MeV)	300	240	272
S_0 (MeV)	32.5	32.5	37.4
L (MeV)	94	90	118
B/A (MeV)	−16.3	−16.3	−16.3

that [22]

$$\frac{g_{YY\sigma}}{g_{NN\sigma}} = 0.7, \quad \frac{g_{YY\omega}}{g_{NN\omega}} = \chi_\omega \quad \frac{g_{YY\rho}}{g_{NN\rho}} = \frac{I_{3B}}{I_{3N}}\chi_\rho, \tag{16}$$

where $\chi_\omega = \chi_\rho$ has the values 0.783 in GM1, 0.8 in GM3, and 0.772 in NL3 in order to describe the well-known $U_\Lambda = -28$ MeV. The hyperon potential depth is defined as [3,19]

$$U_Y = g_{YY\omega}\omega_0 + g_{YY\phi}\phi_0 - g_{YY\sigma}\sigma_0. \tag{17}$$

Note that within the GC parametrization the ρ meson always couples to the isospin projection I_3. Nevertheless, the value of χ_ρ is completely arbitrary [3].

Another possible approach is the assumption of a complete SU(3) symmetry group theory to determine the coupling constants of baryons with all mesons (a detailed calculation is present in the Appendix). We also assume $z_v = \sqrt{6}$ and $\theta_v = 35.264$, in agreement with the SU(6) parametrization of the vector mesons, and a *near* SU(6), with $z_s = \frac{8}{9}\sqrt{6}$ and $\theta_s = 35.264$ for the scalar mesons. Within this complete SU(3) symmetry group model, the hyperon-meson couplings now become

$$\frac{g_{\Lambda\Lambda\omega}}{g_{NN\omega}} = \frac{4+2\alpha_v}{5+4\alpha_v}, \quad \frac{g_{\Sigma\Sigma\omega}}{g_{NN\omega}} = \frac{8-2\alpha_v}{5+4\alpha_v}, \quad \frac{g_{\Xi\Xi\omega}}{g_{NN\omega}} = \frac{5-2\alpha_v}{5+4\alpha_v}, \tag{18}$$

for the meson ω, and, for the meson ϕ, when it is present,

$$\frac{g_{NN\phi}}{g_{NN\omega}} = \sqrt{2}\left(\frac{4\alpha_v - 4}{5+4\alpha_v}\right), \quad \frac{g_{\Lambda\Lambda\phi}}{g_{NN\omega}} = \sqrt{2}\left(\frac{2\alpha_v - 5}{5+4\alpha_v}\right),$$
$$\frac{g_{\Sigma\Sigma\phi}}{g_{\Lambda\Lambda\omega}} = \sqrt{2}\left(\frac{-2\alpha_v - 1}{5+4\alpha_v}\right), \quad \frac{g_{\Xi\Xi\phi}}{g_{NN\omega}} = \sqrt{2}\left(\frac{-2\alpha_v - 4}{5+4\alpha_v}\right). \tag{19}$$

In the traditional $\sigma\omega\rho$ model we consider that all $g_{BB\phi}$ are equal to zero.

For the meson ρ,

$$\frac{g_{\Sigma\Sigma\rho}}{g_{NN\rho}} = 2\alpha_v, \quad \frac{g_{\Xi\Xi\rho}}{g_{NN\rho}} = -(1-2\alpha_v), \quad \frac{g_{\Lambda\Lambda\rho}}{g_{NN\rho}} = 0, \tag{20}$$

TABLE II. Family of parametrizations and hyperon potential depths for GM1.

$\alpha_v = 1$	$\alpha_s = 1.568$	$g_{NN\omega} = 10.610$	$U_\Sigma = +32$	$U_\Xi = +40$
$\alpha_v = 0.75$	$\alpha_s = 1.251$	$g_{NN\omega} = 10.610$	$U_\Sigma = +29$	$U_\Xi = +39$
$\alpha_v = 0.50$	$\alpha_s = 0.9007$	$g_{NN\omega} = 10.610$	$U_\Sigma = +19$	$U_\Xi = +33$
$\alpha_v = 0.25$	$\alpha_s = 0.5230$	$g_{NN\omega} = 10.610$	$U_\Sigma = +11$	$U_\Xi = +29$
$\alpha_v = 0.0$	$\alpha_s = 0.2859$	$g_{NN\omega} = 10.610$	$U_\Sigma = -2$	$U_\Xi = +22$
GC	–	$g_{NN\omega} = 10.610$	$U_\Lambda = -28$	$U_\Xi = -28$

and for the σ,

$$\frac{g_{\Lambda\Lambda\sigma}}{g_{NN\sigma}} = \frac{10 + 6\alpha_s}{13 + 12\alpha_s}, \quad \frac{g_{\Sigma\Sigma\sigma}}{g_{NN\sigma}} = \frac{22 - 6\alpha_s}{13 + 12\alpha_s}, \quad \frac{g_{\Xi\Xi\sigma}}{g_{NN\sigma}} = \frac{13 - 6\alpha_s}{13 + 12\alpha_s}. \tag{21}$$

When we set $\alpha_v = 1$, we recover the SU(6) parametrization for the vector mesons. In this case, the ω meson couples to hypercharge, while the ρ meson couples to isospin, as proposed by Sakurai [41]. When $\alpha \neq 1$, the ϕ meson couples to the nucleon in the $\sigma\omega\rho\phi$ model. To make sure that the nuclear matter properties are not affected, we reparametrize the $g_{NN\omega}$ as follows:

$$g_{NN\omega}\omega_0 \rightarrow \tilde{g}_{NN\omega}\omega_0 + g_{NN\phi}\phi_\phi, \tag{22}$$

where the left-hand side of Eq. (22) is related to the $\sigma\omega\phi$ model, while the right-hand side is related to the $\sigma\omega\rho\phi$ model. Now, from Eqs. (6) and (7),

$$g_{NN\omega}\sum_B \frac{g_{BB\omega}}{m_v^2} n_B \equiv \tilde{g}_{NN\omega}\sum_B \frac{\tilde{g}_{BB\omega}}{m_v^2} n_B + g_{NN\phi}\sum_B \frac{g_{BB\phi}}{m_\phi^2} n_B. \tag{23}$$

However, since hyperons are not present at the nuclear saturation density, the sum runs only over the nucleons. Also $g_{NN\phi}$ depends on the independent $g_{NN\omega}$ from Eq. (19). Therefore we rewrite Eq. (23) as follows:

$$\frac{g_{NN\omega}^2}{m_v^2} \equiv \frac{\tilde{g}_{NN\omega}^2}{m_v^2} + 2\left(\frac{4\alpha_v - 4}{5 + 4\alpha_v}\right)^2 \frac{\tilde{g}_{NN\omega}^2}{m_\phi^2}. \tag{24}$$

Notice that for each α_v, $\tilde{g}_{NN\omega}$ in the $\sigma\omega\rho\phi$ model on the right-hand side of Eq. (24) is determined in such a way that the right-hand side of that equation reproduces the same value of the left-hand side in the traditional $\sigma\omega\rho$ model. We call the parametrizations of the $\sigma\omega\rho\phi$ model the "like model" (LM) (i.e., GM1LM, GM3LM, etc.) since they predict the same quantities for the nuclear saturation as the original models, although with different parameters. As already pointed out in Ref. [20], the unusual N-ϕ coupling that arises when we break the SU(6) symmetry in the LM are in accordance with the huge strange quark condensate in the nucleon found in lattice gauge simulations [42–44].

TABLE III. Family of parametrizations and hyperon potential depths for GM3.

$\alpha_v = 1$	$\alpha_s = 1.678$	$g_{NN\omega} = 8.712$	$U_\Sigma = +22$	$U_\Xi = +29$
$\alpha_v = 0.75$	$\alpha_s = 1.345$	$g_{NN\omega} = 8.712$	$U_\Sigma = +19$	$U_\Xi = +28$
$\alpha_v = 0.50$	$\alpha_s = 1.012$	$g_{NN\omega} = 8.712$	$U_\Sigma = +19$	$U_\Xi = +33$
$\alpha_v = 0.25$	$\alpha_s = 0.6889$	$g_{NN\omega} = 8.712$	$U_\Sigma = +8$	$U_\Xi = +23$
$\alpha_v = 0.0$	$\alpha_s = 0.3763$	$g_{NN\omega} = 8.712$	$U_\Sigma = +0.2$	$U_\Xi = +18$
GC	–	$g_{NN\omega} = 8.712$	$U_\Lambda = -28$	$U_\Xi = -28$

TABLE IV. Family of parametrizations and hyperon potential depths for GM1LM.

$\alpha_v = 1$	$\alpha_s = 1.568$	$g_{NN\omega} = 10.610$	$U_\Sigma = +32$	$U_\Xi = +40$
$\alpha_v = 0.75$	$\alpha_s = 1.231$	$g_{NN\omega} = 10.514$	$U_\Sigma = +25$	$U_\Xi = +39$
$\alpha_v = 0.50$	$\alpha_s = 0.8229$	$g_{NN\omega} = 10.133$	$U_\Sigma = -5$	$U_\Xi = +32$
$\alpha_v = 0.25$	$\alpha_s = 0.6889$	$g_{NN\omega} = 9.324$	$U_\Sigma = -157$	$U_\Xi = -40$

A. Hyperon-meson couplings and potential depths

According to the calculations developed in the Appendix, we have *a priori* just two free parameters, α_v and α_s. Now we proceed as follows: We give arbitrary values to α_v varying from 1 to 0 and impose that α_s assumes the value that keeps $U_\Lambda = -28$ MeV. The uncertain U_Σ and U_Ξ are then determined only by symmetry properties, without any other phenomenological input. We also display the values for $g_{NN\omega}$, which change within the LM. The results are presented from Table II to Table V.

We see that for the SU(6) symmetry ($\alpha_v = 1$), the Ξ potential arises naturally as strongly repulsive, in accordance with what was suggest in Ref. [19] but in an *ad hoc* way. Also, for the SU(6) parametrization, we obtain $\alpha_s = 1.568$ with GM1 and GM1LM. This value is very close to the 1.496 found in Ref. [35].

When $\alpha_v = 0.25$ with GM1LM and GM3LM, the U_Σ becomes too attractive (-157 MeV with GM1LM and -104 MeV with GM3LM). That happens because when we reduce the α_v, the Σ-σ interaction becomes more and more important with the increase of $g_{\Sigma\Sigma\sigma}$. Moreover, the repulsive channel, which is the combination of the Σ-ω and Σ-ϕ interactions, becomes smaller for smaller α_v. These two combined factors made a stunning attractive Σ potential. We show the effect of such attractive potential in Fig. 1 and Fig. 2 and, since this fact is in disagreement with the experience, these parametrizations are no longer used.

We do not study the effects of hyperons with the NL3 parametrization, because, as we see next, this parametrization is in disagreement with all experimental constraints used in this work.

TABLE V. Family of parametrizations and hyperon potential depths for GM3LM.

$\alpha_v = 1$	$\alpha_s = 1.678$	$g_{NN\omega} = 8.712$	$U_\Sigma = +22$	$U_\Xi = +29$
$\alpha_v = 0.75$	$\alpha_s = 1.367$	$g_{NN\omega} = 8.633$	$U_\Sigma = +20$	$U_\Xi = +31$
$\alpha_v = 0.50$	$\alpha_s = 0.9281$	$g_{NN\omega} = 8.320$	$U_\Sigma = -2$	$U_\Xi = +25$
$\alpha_v = 0.25$	$\alpha_s = 0.2775$	$g_{NN\omega} = 7.182$	$U_\Sigma = -104$	$U_\Xi = -23$

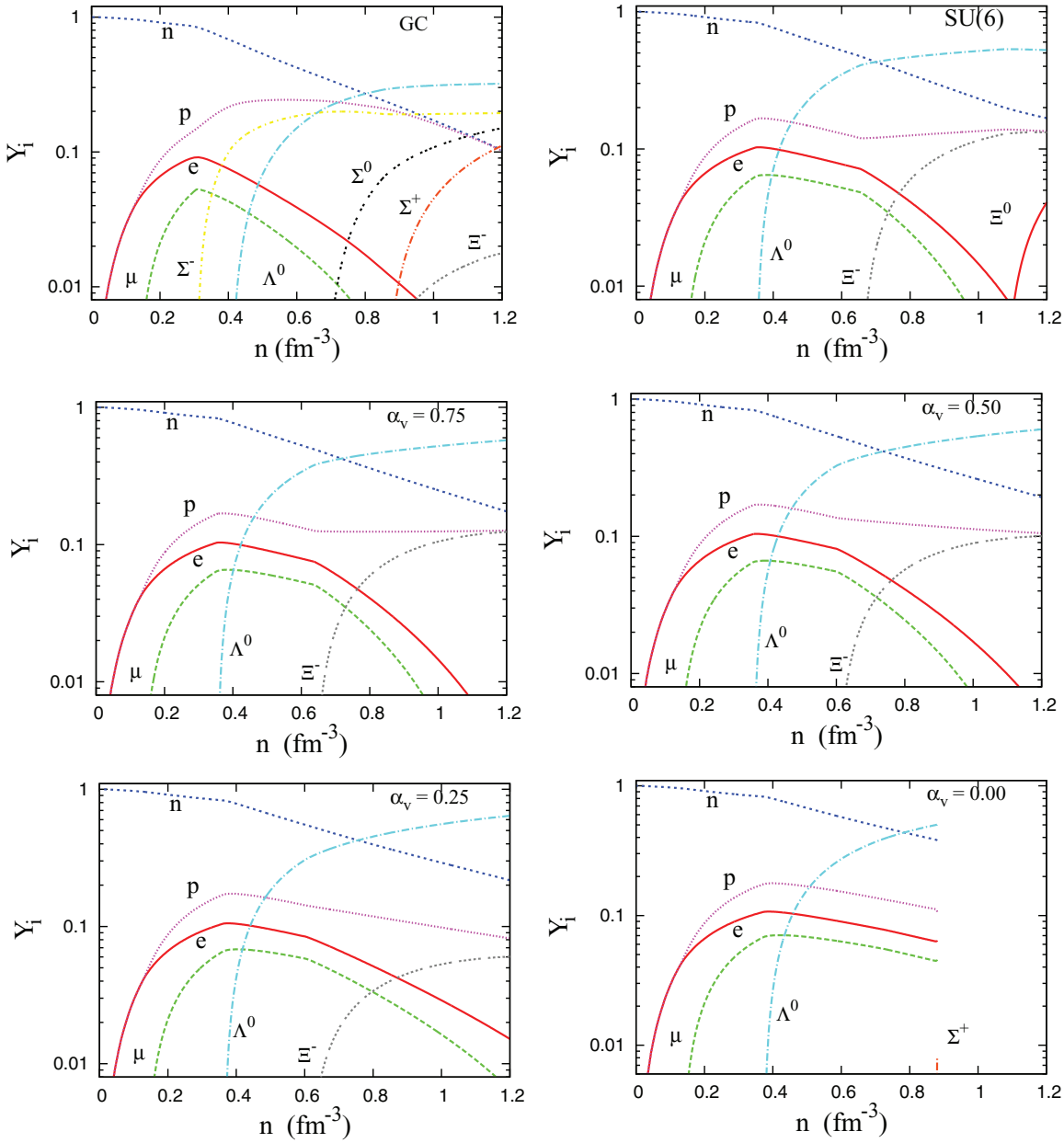

FIG. 1. (Color online) Fraction of particles with the GM1LM parametrization for some different values of α_v.

IV. RESULTS AND CONSTRAINTS

We analyze the hypernuclear matter subject to generalized β equilibrium and electrically neutral conditions. These conditions imply that

$$\mu_i = \mu_n - e_i\mu_i, \quad \mu_e = \mu_\mu, \quad \sum_B n_B e_B + \sum_l e_l + \mu_l = 0, \tag{25}$$

where μ_i and e_i are the chemical potential and the electrical charge of the ith baryon, respectively, while n_B and n_l are the number densities of the baryons and leptons. Notice that in all figures and tables, the SU(6) choice of parameters refers to the case when $\alpha_v = 1$. The fraction of particles is defined as $Y_i = n_i/n$ and we plot them for the GC and several values of α_v with the GM1 parametrization in Fig. 3.

We can see that the GC parametrization differs from all those consistent with the SU(3) symmetry group, since the first hyperon that appears with the GC is the Σ^-, which is absent for all SU(3) parametrizations. Indeed, while all the Σ triplet is present with the GC, this is not the case with the SU(3) choice of couplings, except for the subtle onset of the Σ^+ in $\alpha_v = 0.0$ at large densities. With the SU(3) symmetry, from $\alpha_v = 1.0$, which reproduces the usual SU(6) symmetry choice of parameters, to $\alpha_v = 0.0$, we see that the hyperons are more and more suppressed at high densities due to the increase of the repulsive vector channel. Within SU(6) there are three different hyperons in the composition of the

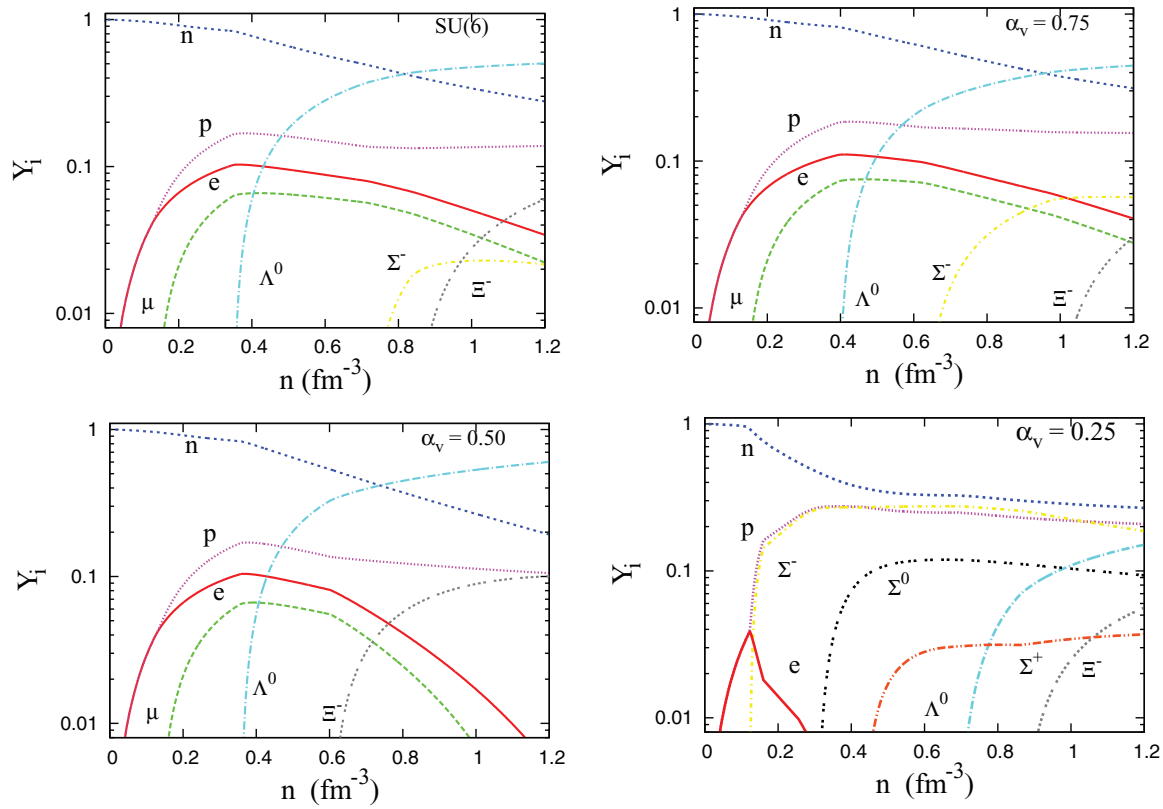

FIG. 2. (Color online) Strangeness fraction for several values of α_v with the GM1 (a) and GM1LM (b) parametrizations. We also include GC parametrization for comparison.

hypernuclear matter, Λ^0, Ξ^-, and Ξ^0. When the value of α_v decreases, the Y-ω interaction becomes stronger, and there is a suppression of the particles with strange content for high density values. The Ξ^0 soon disappears, and the fraction of Ξ^- becomes less relevant at high densities. It is easier to see the hyperon suppression in a plot of the strangeness fraction as shown in Fig. 2. Exactly the same relation between α_v and strangeness, with obvious consequences on the stiffness of the EOS, was found in Ref. [20], an expected behavior since our choice of constants was primordially based on this reference.

We also note that although U_Ξ becomes less repulsive with the decrease of α_v, less hyperons tend to be created. The reason is that both the repulsive vector and the attractive scalar channels increase with the decrease of α_v. When α_v is small, the strong attractive channel dominates for low densities, but the repulsive one dominates at high densities. This creates a weakly repulsive channel at the nuclear saturation point, and the hyperon suppression for densities much above this density. We also note that for $\alpha_v = 0.0$ the code stops converging at not-too-high densities. This fact has already been

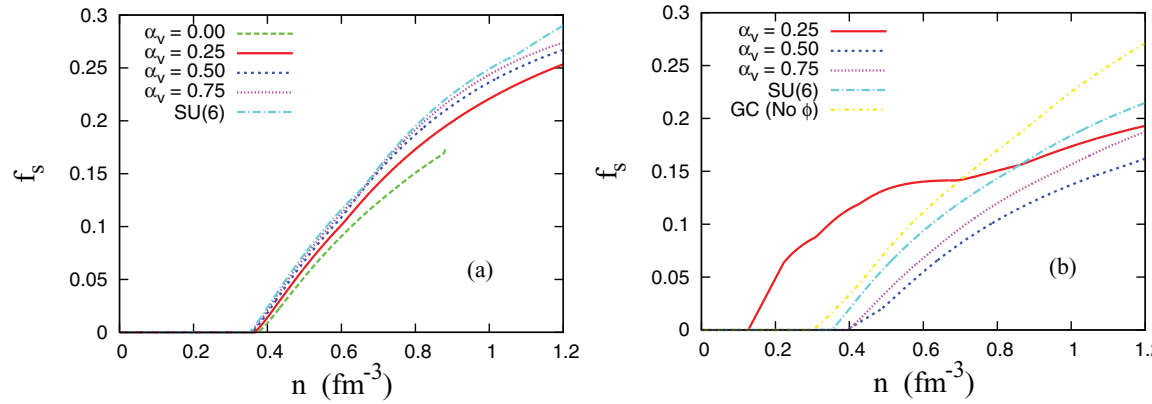

FIG. 3. (Color online) Fraction of particles Y_i, for GC and different values of α_v with the GM1 parametrization. Here $\alpha_v = 1$ refers to the SU(6) usual choice of couplings.

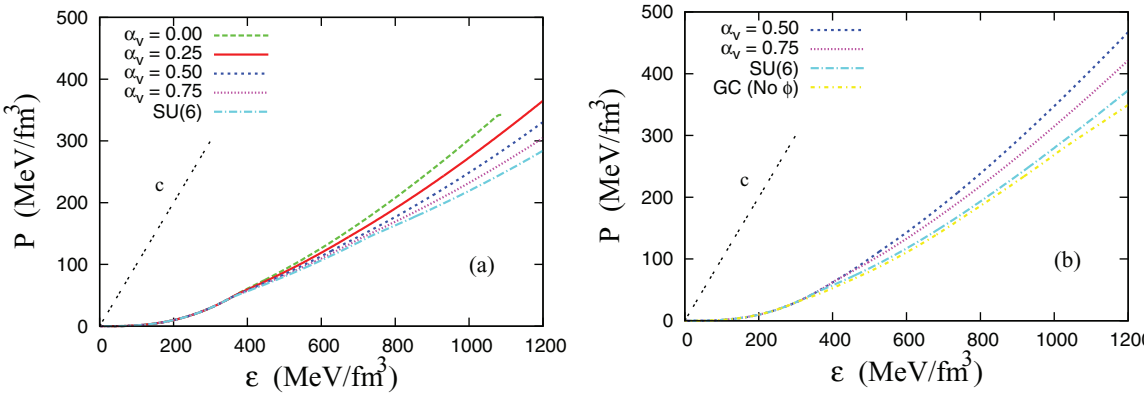

FIG. 4. (Color online) EOS for GM1 (a) and GM1LM (b) for GC and SU(3) group with several values of α_v. The "c" is the causality limit.

discussed in the literature [12,16,29] and occurs because the nucleon effective mass becomes zero. We plot the fraction of particles for the GM1LM in Fig. 1 for different values of α_v.

The main difference between the GM1 and the GM1LM as far as the fraction of particles is concerned refers to the arising of the Σ^-, which appears with the GM1LM and is absent with the GM1, except when we use the GC parametrization. The reason is that the ϕ meson couples more strongly to the Ξ than to the Σ. Also, as an additional source of repulsion, the ϕ meson increase the suppression of hyperons at high densities and easing the production of different particles. With the decrease of α_v, the Σ density onset is lowered. The reason is that the Σ-ϕ coupling becomes weaker and weaker, while the Λ-ϕ coupling becomes stronger. For $\alpha_v = 0.50$, the Σ^- becomes the first hyperon to appear, while for $\alpha_v = 0.25$, the repulsive channel is so weak for the Σ that, alongside the strong attractive channel, the Σ^- arises at the density of 0.13 fm^{-3}, even below the nuclear saturation density. This is the effect of the very low $U_\Sigma = -157$ MeV, which contradicts all physical expectations. As pointed out earlier, the hyperon suppression at high densities with the decrease of α_v, and with the inclusion of the ϕ meson, can be seen best in a plot of the strangeness fraction f_s instead of the individual fraction of particles. f_s is normally defined as

$$f_s = \frac{1}{3}\frac{\sum_i n_i |s_i|}{n}, \tag{26}$$

where s_i is the strangeness of the ith baryon.

For a matter of clarity, so the curves do not overlap, we have decided to plot the curves related to the GC parametrization alongside those of GM1LM, although the ϕ meson is not present in the GC set and is always present in LM.

We see that there is a connection between α_v and f_s. A lower α_v results in a lower f_s both with GM1 and with the GM1LM parametrizations (except when $\alpha_v = 0.25$, GM1LM), due to the strong hyperon suppression at high densities, as already discussed. Moreover, GM1LM produces a lower f_s when compared with the GM1 due to the new vector channel that increases the chemical potential for the hyperons, hindering their production at high densities. In GM1LM when $\alpha_v = 0.25$, the onset of Σ^- at very low densities makes the strangeness fraction nonzero even below the saturation density. Due to this effect, from this point on, we no longer use this parametrization.

One of the most important quantities of nuclear and hypernuclear matter is the EOS. We plot the EOS for the parametrizations discussed above in Fig. 4.

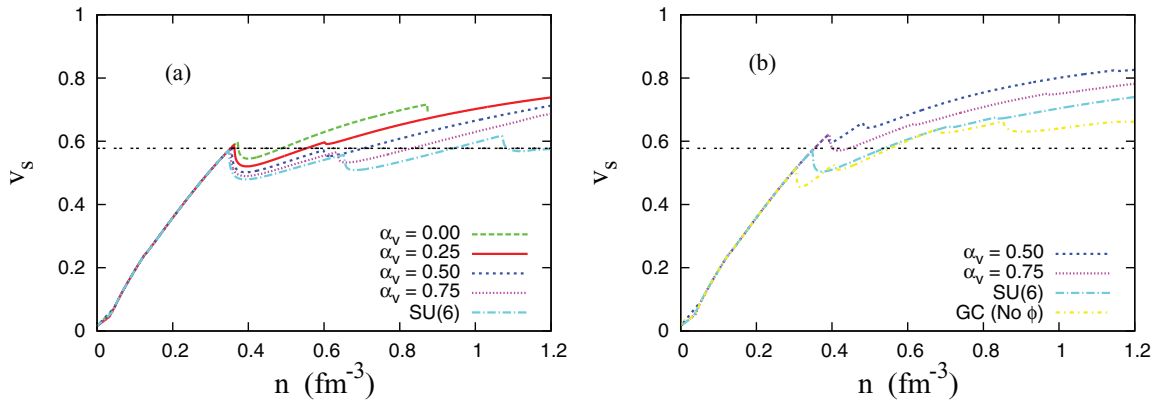

FIG. 5. (Color online) Speed of sound in dense hypernuclear matter for GM1 (a) and GM1LM (b). The horizontal line is the QCD limit of v_s for quark matter.

The relation between α_v and f_s can also be observed in the EOS. Lower values of α_v produce stiffer EOS. This was expected, since lower f_s indicates less hyperons, and the effect of softening of the EOS caused by the hyperons is well known [3,10,13,27]. It is interesting to note that the stiffer EOS is obtained with less repulsive hyperon potentials. This indicates that the influence of the hyperon potential depths as pointed in Ref. [19] is only secondary. The ruling term for the stiffness of the EOS is the strength of the Y-ω interaction. In GM1LM we have alongside the Y-ω interaction the Y-ϕ one. These combined effects produce very stiff EOS, as we can see on the right side of Fig. 4, even for low repulsive hyperon potentials. The "c" line plotted refers to the causality limit. Since our results are derived from a relativistic model, this constraint is never violated.

We have also analyzed the speed of sound v_s, defined as follows:

$$v_s = \sqrt{\left|\frac{\partial p}{\partial \epsilon}\right|}, \tag{27}$$

since it is an important quantity in the study of phase transitions. Although there is no experimental measurement of the speed of sound at high densities, results derived from QCD impose a limit of $v_s = 1/\sqrt{3} \simeq 0.58$ ($c = 1$) for the quark-gluon plasma [45–47]. Methods to measure the speed of sound are proposed in the modern literature [48,49] through Mach cones. Since the density of a possible hadron-quark phase transition is not known, a measure of $v_s > 0.58$ excludes the possibility of quark matter at the densities where such speed is obtained. We plot the speed of sound in Fig. 5.

As expected, the speed of sound is the same for all parametrizations while hyperons are not present. The onset of hyperons reduces the speed of sound due to the softening of the related EOS, resulting in a connection between α_v and v_s. A stiffer EOS, obtained with lower values of α_v, yields a higher value for the speed of sound at high densities.

Without hyperons the breaking of the QCD theoretical limit for the speed of sound occurs at 0.352 fm^{-3}. The main question therefore is in which parametrizations the first hyperon arises below this density. When the first hyperon arises before the density of 0.352 fm^{-3}, the density at which the speed of sound exceeds 0.58 increases substantially. We display in Table VI the density in which the speed of sound surpasses the QCD speed limit for different values of α_v.

We see that for the sets GC, SU(6), $\alpha_v = 0.75$, and $\alpha_v = 0.50$ with the GM1 parametrization and the SU(6) with the GM1LM, the first hyperon appears below 0.352 fm^{-3}, resulting in the fact that the QCD limit of the speed of sound is attained at higher density values. Later, we see that this fact has implications when we analyze some experimental constraints.

A. Constraints

In order to validate our proposal, we confront it with some experimental values and astrophysical observations. The first experimental constraint (which we call EC1) is the asymmetric coefficient S_0 and the symmetry energy slope L as defined in Ref. [50],

TABLE VI. Number density in which the speed of sound exceeds the theoretical limit of QCD for GM1 and GM1LM with different parametrization sets.

Model	α_v	$v_s > 0.58$ at	Model	α_v	$v_s > 0.58$ at
GM1	SU(6)	6.16 n_0	GM1LM	SU(6)	3.51 n_0
GM1	0.75	5.44 n_0	GM1LM	0.75	2.30 n_0
GM1	0.50	4.60 n_0	GM1LM	0.50	2.30 n_0
GM1	0.25	2.30 n_0			
GM1	0.0	2.30 n_0	GM1	GC	3.62 n_0

$$S(n) = S_0 - L\epsilon + \frac{1}{2}K_{\rm sym}\epsilon^2 + O(\epsilon^3), \tag{28}$$

$$\epsilon = \frac{n_0 - n}{3n_0}, \quad \text{and} \quad L = 3n_0\frac{dS}{dn}\bigg|_{n_0}. \tag{29}$$

The values of S_0 and L for GM1, GM3, and NL3 are given in Table I. We analyze these tree parametrizations in the light of two experimental data described in Ref. [50], obtained from heavy-ion collision (HIC, hatched area in green) and isobaric analog states (IAS, hatched area in pink). The experimental values of S_0 and L and the theoretical predictions obtained with GM1, GM3, and NL3 are presented in Fig. 6.

We see that while GM1 and GM3 agree with both experimental measurements, the NL3 parametrization is completely out of the allowed region. Since we expect that neutron stars are neutron-rich systems, the symmetry energy plays a crucial role in the description of these objects. Because the NL3 parametrization is in disagreement with the experimental observation, this parametrization should be avoided, at least in the description of neutron star properties.

The second experimental constraint (EC2) is the nucleon potential in symmetric matter. From measurements of kaon production in HIC performed with the kaon spectrometer (KaoS) [30], an upper limit was established to at least 2 times the nuclear saturation density. In QHD-based models the

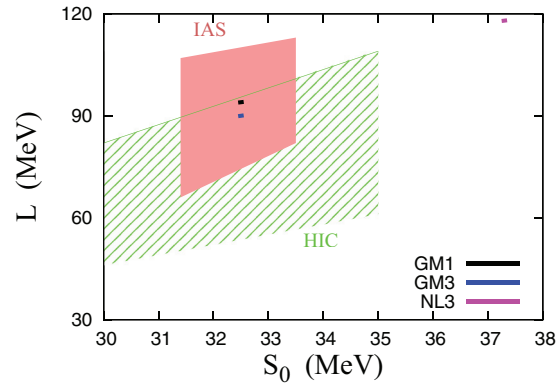

FIG. 6. (Color online) EC1: S_0 and L experimental values obtained for HIC and IAS and the prediction of the GM1, GM3, and NL3 parametrizations.

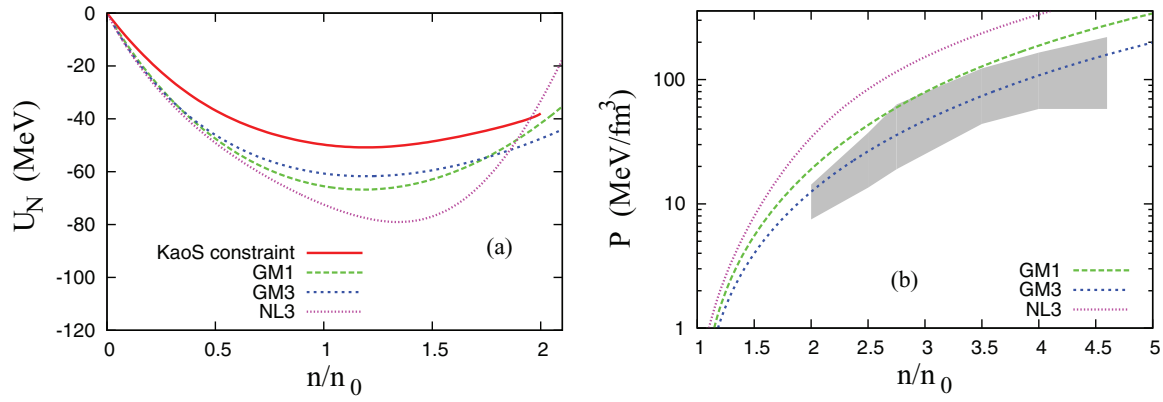

FIG. 7. (Color online) EC2 (a): Experimental value of U_N from kaon production up to 2 times the saturation point ($n_0 = 0.153$ fm^{-3}). EC3 (b): Experimental determination of the pressure in symmetric nuclear matter.

nucleon potential in symmetric matter is defined as follows:

$$U_N = g_{NN\omega}\omega_0 - g_{NN\sigma}\sigma_0. \tag{30}$$

The third experimental constraint (EC3) is the pressure of symmetric nuclear matter up to almost five times the nuclear density as obtained in Ref. [31]. The predictions obtained with GM1, GM3, and NL3 and the experimental upper limit of the nucleon potential withdrawn from Ref. [30] are plotted in Fig. 7(a), and the pressure (hatched area) is from Ref. [31] and the predictions are plotted in Fig. 7(b).

Both constraints point towards the same direction: The EOS must be soft for densities not much above the nuclear saturation point. Wee see that NL3 fails again when confronted with the EC2 and EC3. On the other hand, GM3 fulfills all the experimental constraints we have analyzed. The GM1 parametrization presents a more delicate situation. While GM1 is in accordance with EC1 and EC2, it fails to describe EC3. So, at first glance, this parametrization should be be ruled out. However, as pointed out in Ref. [31], the experimental results do rule out neither hyperon creation nor even more exotic pictures, such as quark-hadron phase transitions. The softening of the EOS due to the hyperon onset could be the key to reconcile experiment and theory.

Note that in symmetric nuclear matter, the chemical potential of the protons is equal to the chemical potential of the neutron. Now we define the hypernuclear symmetric matter, imposing that the hyperon chemical potential be equal to the chemical potential of the nucleons,

$$\mu_Y = \mu_p = \mu_n. \tag{31}$$

This choice implies that only symmetric nuclear matter exists until the density is high enough so the creation of strange particles becomes energetically favorable, softening the EOS. We plot the pressure of hypernuclear symmetric matter alongside the experimental constraint EC3 (hatched area) in Fig. 8.

We see that for $\alpha_v = 1$, $\alpha_v = 0.75$, and $\alpha_v = 0.50$ with GM1, and the SU(6) parametrization with GM1LM, the prediction of pressure falls again in the experimental area at high densities. It is interesting to note that the normally used GC parametrization fails to reproduce the experimental constraint and, therefore, should be taken with care.

As pointed out earlier, the speed of sound has implications which relate to the EC3. With the exception of the GC, all parametrization sets that agree with the EC3 break the QCD theoretical limit of the speed of sound for densities above 3 times the nuclear saturation density. Moreover, according to our proposal, all parametrization sets that agree with the EC3 have the Λ^0 as the first hyperon that arises, and its onset needs to occur at densities below 0.352 fm^{-3}.

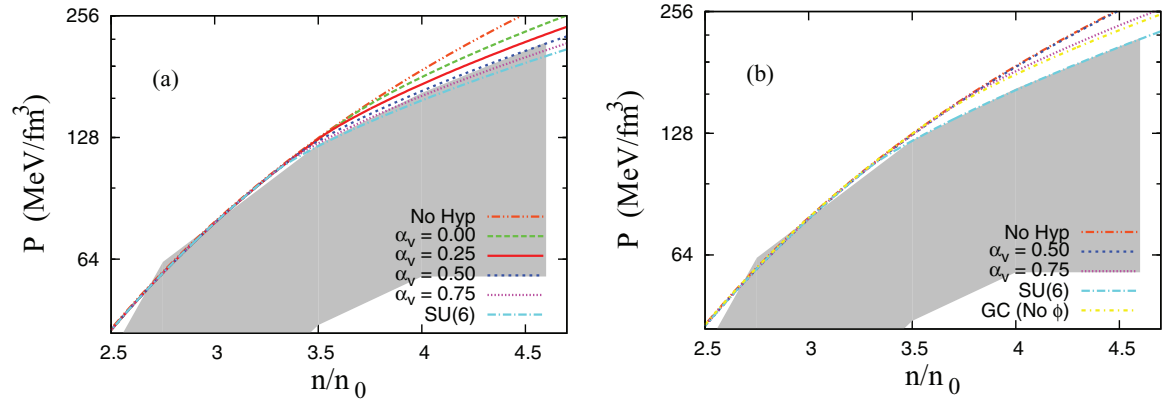

FIG. 8. (Color online) Pressure of hypernuclear symmetric matter in GM1 (a) and GM1LM (b) parametrizations for different values of α_v.

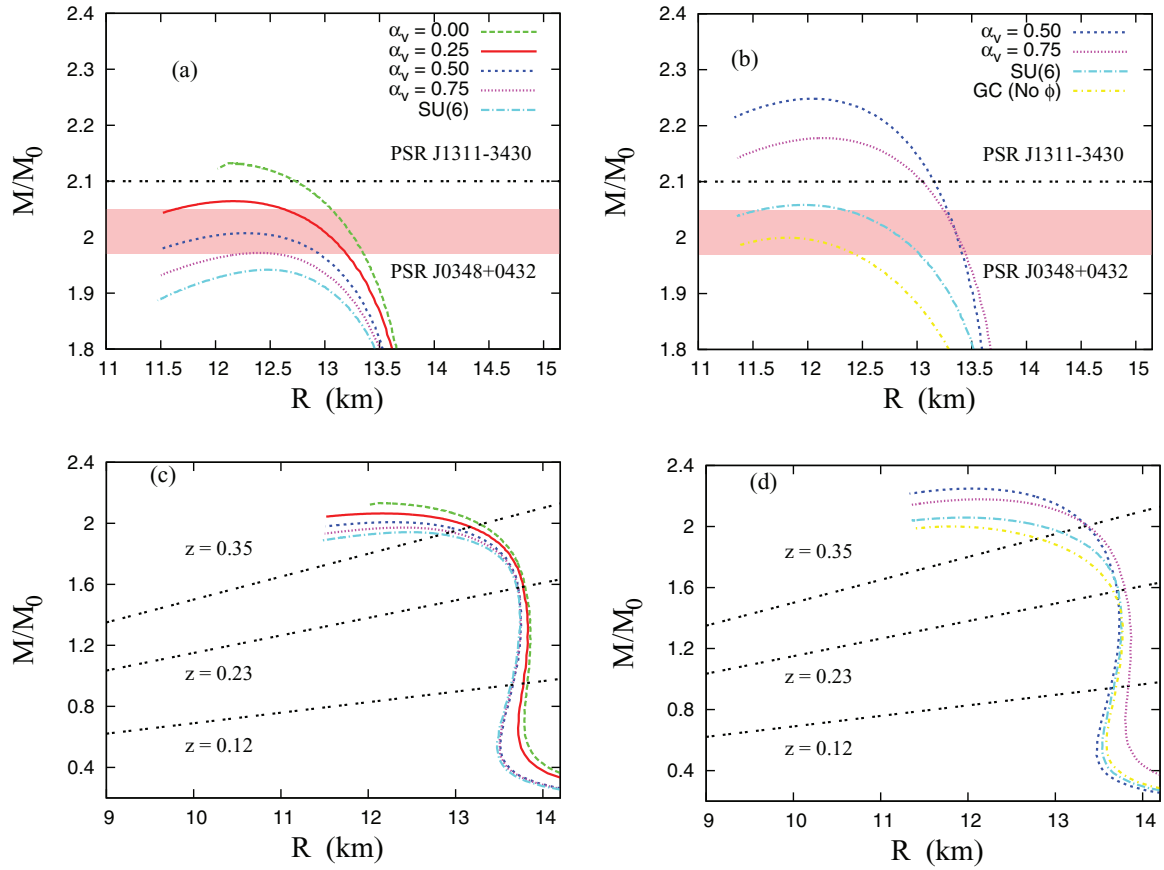

FIG. 9. (Color online) Mass-radii ratio for GM1 [(a) and (c)] and GM1LM [(b) and (d)], emphasizing the AC1 (above) and the AC2 (below).

It is also important to note that although some of the GM1 and GM1LM hypernuclear parametrizations are in agreement with the experimental data for high densities, they are still in disagreement at low densities. However, this could be due to the fact that we ignore meson production, which is important at subthreshold densities, as pointed out in Refs. [30,51].

Now we turn towards the constraints obtained from astrophysical observations. The main constraints are the recent observations of the two massive pulsars, PSR J1614-2230 [1] and PSR J0348+0432 [2], which indicate that the EOS has to be stiff enough to reproduce 2 $M_\odot$ neutron stars. Therefore, we have two, in principle, contradictory constraints for low and high densities: The experimental ones point to a soft EOS at low densities [30,31], and the astrophysical observations favor a stiff EOS at high densities [1,2]. We next check all parametrizations discussed so far to see whether they can fulfill these two features. The mass of the PSR J0348+0432 is $2.01 \pm 0.04\ M_\odot$, and we use this value as the first astrophysical constraint (AC1). The second astrophysical constraint (AC2) is the redshift measurements (z) of two neutron stars. A redshift of $z = 0.35$ has been obtained from three different transitions of the spectra of the EXO0748-676 [52]. This redshift corresponds to $M/R = 0.15\ M_\odot$/km. Another constraint on the mass-radius relation comes from the observation of two absorption features in the source spectrum of the 1E 1207.4-5209 neutron star, with redshift from $z = 0.12$ to $z = 0.23$, which gives $M/R = 0.069\ M_\odot$/km to $M/R = 0.115\ M_\odot$/km [53].

It is also worth mentioning that, recently, the existence of a 2.7 solar mass object named PSR J1311-3430 [54] was suggested. Although such a hypermassive pulsar is not confirmed yet, all previous measurements indicate a lower limit of 2.1 $M_\odot$. We use this value as a possible constraint.

To check which EOS is hard enough to reproduce the well-known PSR J0348+0432 and which one also agrees with the redshift measurements, we solve the Tolman-Oppenheimer-Volkoff equations [55], which are the differential equations for the structure of a static, spherically symmetric, relativistic star in hydrostatic equilibrium. Also, we use the BPS [56] EOS for the very low density regime to simulate the neutron star crust. We plot the results for GM1 and GM1LM for several values of α_v and the GC parametrization in Fig. 9. The properties of the maximum mass of each parametrization are displayed in Table VII.

From Fig. 9 and Table VII, one can see that the only parametrization that fails to describe the AC1 is GM1 with the SU(6) choice of couplings. All other parametrizations both in GM1 and in GM1LM yield a maximum mass of at least 1.97 $M_\odot$. All models are in agreement with AC2. On the other hand, the speculative PSR J1311-3430 [54] is described only by few parametrizations: $\alpha_v = 0.0$ with GM1 and $\alpha_v \leqslant 0.75$ with GM1LM are able to explain such high mass. Nevertheless, all

TABLE VII. Stellar properties obtained with GM1 and GM1LM parametrizations with GC and different values of α_v.

Model	α_v	$M/M_\odot$	R (km)	n_c (fm^{-3})	f_s at n_c.
GM1	No hyp.	2.39	11.99	0.840	0.00
GM1	SU(6)	1.94	12.48	0.836	0.206
GM1	0.75	1.97	12.40	0.848	0.206
GM1	0.50	2.00	12.28	0.867	0.206
GM1	0.25	2.06	12.16	0.885	0.196
GM1	0.0	2.13	12.09	0.891	0.178
GM1	GC	2.01	11.86	0.952	0.231
GM1LM	SU(6)	2.06	11.96	0.915	0.168
GM1LM	0.75	2.17	12.13	0.875	0.135
GM1LM	0.50	2.25	12.04	0.870	0.117

parametrization sets that can explain a pulsar with 2.1 $M_\odot$ yield a very stiff EOS, in disagreement with expected low-density constraints [31].

In Ref. [20], the authors propose a linear relation between the maximum mass and the strangeness fraction. In this work, as we see from Table VII, this relation is not present. However, a very interesting result turns up: all the parametrizations that are in agreement with the experimental constraint EC3, obtained from Ref. [31], yield exactly the same strangeness fraction of 0.206 in the GM1 model. In the GM1LM just one agrees with the EC3, the SU(6) parametrization set, which produces a value of $f_s = 0.168$.

It is also interesting to note that the trick of adding a new repulsive meson ϕ to stiffen the EOS indeed reproduces more massive neutron stars. However, the price we pay is that most of the parametrizations with the GM1LM present very high pressure, which is in conflict with EC3. As we have already said, the SU(6) is the only parametrization that conciliates EC3 with GM1LM. Moreover, observing Fig. 8(b), we see that the SU(6) parametrization is in the upper limit of the pressure that remains in accordance with EC3. This strongly constraints the maximum allowed mass value around 2.06 $M_\odot$, at least in mean-field QHD-based models with our choice of couplings. As pointed out earlier, the best parametrization that describes the experimental constraints is the GM3. Without hyperons, this parametrization predicts a neutron star with a mass of 2.04 $M_\odot$, in agreement with all constraints analyzed at all densities. Nevertheless, this parametrization rules out hyperon in neutron star cores, since no value of α_v is able to predict hyperonic neutron stars with masses larger than 1.91 $M_\odot$, as show in Fig. 10.

The third astrophysical constraint (AC3) is a theoretical one. Based on chiral effective theory, Ref. [57] constrains the radii of the canonical 1.4 $M_\odot$ neutron star to 9.7–13.9 km. We plot in Table VIII the minimum and the maximum radii of the canonical mass for different models and parametrizations.

We see that although close to the theoretical limit, the GM1 and GM1LM agree with Ref. [57]. GM3 and GM3LM also agree with AC3, but, as noted before, are in disagreement with AC1 if hyperons are present. NL3 agrees with AC1 and AC2 but fails again when confronted with AC3.

The physics of neutron stars radii has evolved significantly in the past few years and we are now aware that neutron stars radii are certainly correlated with the symmetry energy slope L [16,58,59]. Although we have used Ref. [50] as our main reference for the symmetry energy and its slope, and Ref. [57] to constrain the neutron star radii, other studies exhibit more restricted values for both the slope and neutron star radius. In Refs. [60,61] the slope L is predicted to lie below 62 MeV, a much lower value than the ones of the GM1 and GM3 parametrizations used in the present work (see Table I). In Refs. [60,62] a limit of 12 km for the radius of the canonical 1.4 $M_\odot$ neutron star was obtained, while in Ref. [61] the limit is 13.1 km, closest to what was achieved in our work. Also, recently, two different analyses of five quiescent low-mass x-ray binaries in globular clusters resulted in different ranges for neutron star radii. While one of them, in which it was assumed that all neutron stars have the same radii, predicted that they should lie in the range $R = 9.1^{+1,3}_{-1.5}$ [63], another calculation, based on a Bayesian analysis, foresees radii of all neutron stars to lie in between 10.9 and 12.7 km [64], which would put all predictions of our models in conflict with the experimental data for the canonical 1.4 $M_\odot$ neutron stars. However, as pointed out by the authors, better x-ray data are needed to determine the compositions of accreting neutron

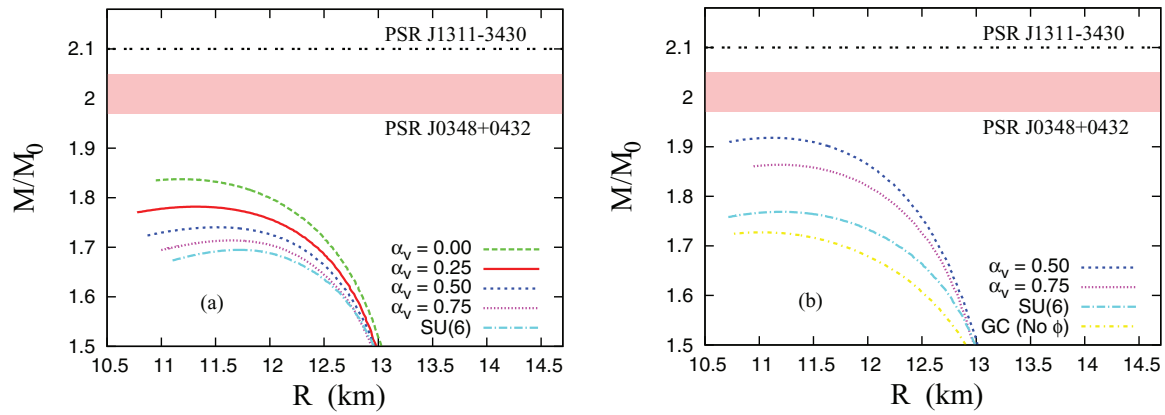

FIG. 10. (Color online) Neutron stars mass-radii relation for GM3 (a) and GM3LM (b). No parametrization is able to predict the mass of PSR J0438+0432.

TABLE VIII. Minimum and maximum radii of the canonical 1.4 $M_\odot$ for different models and parametrizations.

Model	Min./Max. radii (1.4 $M_\odot$).	AC3
GM1,GM1LM	13.73/13.85 km	OK
GM3,GM3LM	13.06/13.14 km	OK
NL3	14.71 km	Failed

stars, as this can make changes of 30% or greater in inferred neutron star radii [64].

There are other parametrizations within QHD models with values of the symmetry energy and slope that lie within the ones advocated in Ref. [61], i.e., $29 < S_0 < 32.7$ MeV and $40.5 < L < 61.9$ MeV. The FSU [65] (also known) as FSUGold and IUFSU [66] parametrizations, for instance, yield values for S_0 equal to 32.6 and 31.3 MeV and for L equal to 60.5 and 47.2 MeV, respectively. However, although these model calculations result in low radii (12.41 km for the FSU and 12.55 km for the IU-FSU [16]), they are unable to explain the recent super massive pulsars [1,2]. The maximum mass is 1.73 $M_\odot$ [67] with FSU (also called FSU1.7 in Ref. [67]) and 1.95 $M_\odot$ with IUFSU [16]. In Ref. [67] a 2.1 $M_\odot$ star was obtained with the inclusion of an additional term to the pressure in an *ad hoc* way and the parametrization was renamed FSU2.1 but it did not succeed in explaining a low radius, since the radius of the 1.4 $M_\odot$ is 14 km, a value which is very close to the ones obtained with the GM1 and GM1LM parametrizations. Moreover, it is worth bearing in mind that the low mass achieved with the FSU and IUFSU models are obtained without hyperons. When we allow hyperons to populate the neutron star core, the EOS becomes softer and the maximum mass decreases, as in any of these QHD models. With the SU(6) parametrization, the maximum mass drops to 1.37 $M_\odot$ and 1.55 $M_\odot$ respectively for FSU and IUFSU [16]. With FSU not even the canonical 1.4 $M_\odot$ can be obtained. With the SU(3) symmetry, the masses increase but not enough to achieve masses above 1.8 $M_\odot$. Hence, for the present work, we see no reason to go deeper into these models.

On the other hand, we can reduce the slope and the neutron star radii decreasing the symmetry energy without affecting any of the properties of symmetric nuclear matter by lowering the coupling constant $g_{NN\rho}$ [3]. By fitting the symmetry energy to 30.5 MeV instead of 32.5 with GM1 and GM1LM, we reduce the slope L from 94 to 88 MeV and the neutron star radii drops 0.1 km. With GM3 and GM3LM the slope is reduced from 90 to 84 MeV, while the neutron star radii drops 0.07 km. In both cases, the improvement is only modest and the maximum masses are not affected. Of course, even lower values of the symmetry energy produces lower values of the slope and neutron star radii and we have to remember that the EC1 constrains the limit of the symmetry energy to 30 MeV.

We believe that definite values for the neutron star radii and the slope of the symmetry energy are not yet established. While the previous discussion indicates a low radii, RX J1856.5-3754 may have a radius of 17 km [68]. Some not completely discarded studies indicate that the slope value can reach 113 MeV [69].

TABLE IX. Our choice of the parametrizations when confronted with experimental and observational constraints.

Model	α_v	EC1	EC2	EC3	AC1	AC2	AC3
GM1	No hyp.	OK	OK	Failed	OK	OK	OK
GM1	SU(6)	OK	OK	Fair	Failed	OK	OK
GM1	0.75	OK	OK	Fair	OK	OK	OK
GM1	0.50	OK	OK	Fair	OK	OK	OK
GM1	0.25	OK	OK	Failed	OK	OK	OK
GM1	0.0	OK	OK	Failed	OK	OK	OK
GM1	GC	OK	OK	Failed	OK	OK	OK
GM1LM	SU(6)	OK	OK	Fair	OK	OK	OK
GM1LM	0.75	OK	OK	Failed	OK	OK	OK
GM1LM	0.50	OK	OK	Failed	OK	OK	OK
GM3	No hyp.	OK	OK	OK	OK	OK	OK
GM3	All/GC	OK	OK	OK	Failed	OK	OK
GM3LM	All	OK	OK	OK	Failed	OK	OK
NL3	No hyp.	Failed	Failed	Failed	OK	OK	Failed
FSU	No hyp.	OK	OK	OK	Failed	OK	OK
IU-FSU	No hyp.	OK	OK	OK	Failed	OK	OK

Another astrophysical constraint is related to the maximum possible neutron star mass. According to Ref. [70], it must be lower than 3.2 $M_\odot$ independently of the choice of the EOS. This theoretical constraint was updated in Ref. [30], where the maximum mass around 3.0 $M_\odot$ was found due to the weakly repulsive nucleon potential. In our work the maximum mass is obtained with NL3 without hyperons and is equal to 2.81 $M_\odot$. So all our models are in agreement with the maximum possible neutron star masses [30,70].

Finally, we resume our main results in Table IX, indicating the way each parametrization behaves when confronted with the six constraints used in this work. The concept *Fair* that appears in Table IX is due to the fact that the parametrization agrees with the EC3 at high densities, but continues to fail at low densities as pointed in Fig. 7.

V. CONCLUSION

In this work we investigated the hyperon onset in hypernuclear matter imposing a complete SU(3) symmetric model, where we propose that all hyperon-meson couplings need to obey the SU(3) symmetry properties in order to reduce the number of free parameters of the theory. Utilizing a QHD-based model, we analyze three widely used parametrizations, GM1, GM3, and NL3, in two different models, which we refer to as $\sigma\omega\rho$ and $\sigma\omega\rho\phi$. We then test them against experimental and astrophysical constraints obtained in the past decade. We see that NL3, although it describes nuclear matter properties very well, fails to describe dense asymmetric matter. Also, although we can predict very massive hyperonic stars with many of the investigated parametrizations, a maximum mass of 2.06 $M_\odot$ arises in order to describe the soft EOS in the low-density regime. This constraint prevents us from explaining the mass of the speculative PSR J1311-3430 since none of the parametrizations that agree with EC3 can reproduce such a high mass.

With the GM1LM, the trick of adding a new vector meson in order to stiff the EOS seems to be valid only if the SU(6) choice

of couplings is used. Lower values of α_v enters in conflict with EC3. Also, if we assume that GM1 is a good parametrization to describe nuclear properties, this implies that the hyperon production is not only possible but also necessary to soften the EOS and reconcile theory and experience.

We also analyze some theoretical features of the model, as the speed of sound in dense nuclear matter. We see that stiffer EOS have also higher value of v_s. Since there exists a theoretical limit for the speed of sound in quark matter, a measurement of this physical quantity may be important to rule out quark-hadron phase transitions at specific densities. Also, an unexpected relation arises when we compare the speed of sound with the EC3, which ultimately constraints the hyperon onset.

The possibility of a linear relation between the maximum stellar mass and the strangeness fraction found in Ref. [20] was also investigated for the present choice of parameters. Within our prescription, we do not see this relation.

The role of the hyperon potential as proposed in Ref. [19] was also checked and we found that less repulsive potentials produce stiffer EOS. This is due to the fact that the vector meson channel dominates at high densities, and the role of hyperon potentials plays only a secondary role.

Despite all the efforts made in recent years toward a better understanding of nuclear matter and its implication in neutron star properties, there is still much work to be done. The possibility of a hypermassive 2.7 $M_\odot$ neutron star [54] and very compact ones [63,64] are examples of still-unexplained phenomena.

The consequences of considering the scalar-isovectorial δ meson are the next step of the present work. The ω-ρ interaction present in the FSU and IUFSU models can be added to the models discussed in the present work and its strength adjusted as in Refs. [16,59] so the symmetry energy slope can be reduced. While in the present work only vector strange mesons were considered, strange scalar mesons can also be added to specific parametrizations so a stellar maximum mass of 2.06 $M_\odot$ can be attained, as shown in Ref. [71]. Also, as pointed out in the literature [28,72,73], effects of a strong magnetic field could be important in the description of magnetars. Works along these lines are in progress.

ACKNOWLEDGMENTS

This work was partially supported by CAPES, CNPq, and FAPESC. We thank Luis B. Castro for his patience in checking some FORTRAN codes and for pointing out some ambiguities in the manuscript.

APPENDIX: SU(3) SYMMETRY GROUP

In order to consider a completely symmetric theory for the strong interaction based on a QHD model, we impose that the Yukawa-type interaction is invariant under SU(3) transformations. In what follows we just consider the electric coupling since the magnetic coupling does not contribute in a mean-field approximation [74]. The Yukawa interaction is expressed as follows [75]:

$$\mathcal{L}_{\rm YUK} = -g(\bar{\psi}_B\psi_B)M, \tag{A1}$$

where ψ_B is the Dirac field of baryons and M is the field of an arbitrary meson. This Lagrangian belongs to the irreducible representation IR{1}, a unitary singlet. All the baryons of the model we consider belong to IR{8}. The mesons of the vector IR{8} are the ω_8 and ρ^0. ϕ_1 is a vector singlet, σ_8 belongs to the IR{8} of the scalar octet, and σ_1 is a scalar singlet. Now, to preserve the unitary symmetry, $(\bar{\psi}_B\psi_B)$ must transform as follows: IR{8} when M belongs to IR{8} and IR{1} when M belongs to IR{1}.

However, by use of the Speiser method [75], there are two ways to couple {8} $\otimes$ {8} to {8}, typically the symmetric and the antisymmetric ones [76]. Therefore, the Yukawa interaction can be written as follows:

$$\mathcal{L}_{\rm YUK} = -\left(g_1^8\mathcal{C}^1 + g_2^8\mathcal{C}^2\right)(\bar{\psi}_B\psi_B)M, \tag{A2}$$

for the mesons belonging to IR{8}, and

$$\mathcal{L}_{\rm YUK} = -(g^1)M, \tag{A3}$$

for the mesons belonging to IR{1}, where $\mathcal{C}^1$ and $\mathcal{C}^2$ are the SU(3) Clebsch-Gordan (CG) coefficients of the symmetric and antisymmetric coupling respectively. In this work we use the CG as in Ref. [77]. Following Ref. [75] we introduce the following constants:

$$g_8 = \left[\sqrt{30}/40 g_1^8 + (\sqrt{6}/24)g_2^8\right] \text{ and } \alpha = (\sqrt{6}/24)\left(g_2^8/g_8\right), \tag{A4}$$

which allow us to write the coupling constants of the baryons with the vector mesons as follows:

$$\begin{aligned}
&g_{NN\rho} = g_{8v}, \quad g_{\Sigma\Sigma\rho} = 2g_{8v}\alpha_v, \quad g_{\Xi\Xi\rho} = -g_{8v}(1-2\alpha_v),\\
&g_{\Lambda\Lambda\rho} = 0, \quad g_{NN\omega_8} = \tfrac{1}{3}g_{8v}\sqrt{3}(4\alpha_v - 1),\\
&g_{\Sigma\Sigma\omega_8} = \tfrac{2}{3}g_{8v}\sqrt{3}(1-\alpha_v), \quad g_{\Xi\Xi\omega_8} = -\tfrac{1}{3}\sqrt{3}g_{8v}(1+2\alpha_v),\\
&g_{\Lambda\Lambda\omega_8} = -\tfrac{2}{3}g_{8v}\sqrt{3}(1-\alpha_v),\\
&g_{NN\phi_1} = g_{\Sigma\Sigma\phi_1} = g_{\Lambda\Lambda\phi_1} = g_{\Xi\Xi\phi_1} = g_{1v},
\end{aligned} \tag{A5}$$

while the couplings with the scalar ones read as follows:

$$\begin{aligned}
&g_{NN\sigma_8} = \tfrac{1}{3}g_{8s}\sqrt{3}(4\alpha_s - 1), \quad g_{\Sigma\Sigma\sigma_8} = \tfrac{2}{3}g_{8s}\sqrt{3}(1-\alpha_s),\\
&g_{\Xi\Xi\sigma_8} = -\tfrac{1}{3}\sqrt{3}g_{8s}(1+2\alpha_s), \quad g_{\Lambda\Lambda\sigma_8} = -\tfrac{2}{3}g_{8s}\sqrt{3}(1-\alpha_s),\\
&g_{NN\sigma_1} = g_{\Sigma\Sigma\sigma_1} = g_{\Lambda\Lambda\sigma_1} = g_{\Xi\Xi\sigma_1} = g_{1s},
\end{aligned} \tag{A6}$$

where the new subscripts v and s appear to differentiate the set of vector mesons from the set of the scalar ones. Also, all the constructions that couple baryons of different species are ignored.

In nature, the observed ω and ϕ mesons are not the theoretical ω_8 and ϕ_1 ones but a mixture of them [24]. So, the coupling constants of the real vector mesons with the baryons read as follows:

$$\begin{aligned}
g_{NN\omega} &= \cos\theta_v g_{1v} + \sin\theta_v \tfrac{1}{3}\sqrt{3}g_{8v}(4\alpha_v - 1),\\
g_{\Sigma\Sigma\omega} &= \cos\theta_v g_{v1} + \sin\theta_v \tfrac{2}{3}\sqrt{3}g_{8v}(1-\alpha_v),\\
g_{\Lambda\Lambda\omega} &= \cos\theta_v g_{1v} - \sin\theta_v \tfrac{2}{3}\sqrt{3}g_{8v}(1-\alpha_v),\\
g_{\Xi\Xi\omega} &= \cos\theta_v g_{1v} - \sin\theta_v \tfrac{2}{3}\sqrt{3}g_{8v}(1+2\alpha_v).
\end{aligned} \tag{A7}$$

The results for the ϕ coupling are similar, just replacing $\cos\theta_v \to -\sin\theta_v$ and $\sin\theta_v \to \cos\theta_v$ [24]. In the case of the real scalar mesons $\epsilon(760)$ (what we call here just σ) and the $f_0(980)$ (call here σ^*) [36], the procedure is entirely analogous to the ω and ϕ, respectively, just replacing ω by σ, ϕ by σ^*, and the subscript v by s in Eq. (A7). In order to obtain stiffer EOS the σ^* meson is not considered as in Refs. [19,20].

Since the meson nucleon parametrization is fixed, we have *a priori* six free parameters: $z_v = (g_{8v}/g_{1v})$, θ_v, α_v, $z_s = (g_{8s}/g_{1s})$, θ_s, and α_s. To reduce the numbers of free parameters, for the vector mesons, we use the hybrid SU(6) symmetry group [36,76] to fix the $z_v = \sqrt{6}$ and $\theta_v = 35.264$, which correspond to an ideal mixing angle. This leaves just α_v as a free parameter. When $\alpha_v = 1$, we recover the complete SU(6) parametrization for the vector mesons coupling [21]. This approach based on the SU(6) symmetry for the vector mesons is widely accepted in the literature [19,20,24,74,78,79].

On the other hand, for the scalar mesons the literature is controversial. In Ref. [36] the σ meson is considered a member of IR$\{8\}$, while in Refs. [78,79] it is considered a true member of IR$\{1\}$. In Ref. [80], the σ meson is taken as the mixing of not two but three scalar mesons. Finally, in Refs. [35,37] an almost ideal mixing is assumed. We follow the last prescription and consider $\theta_s = 35.254$ as an ideal mixing approximation. For the z_s, we use a *near SU(6) symmetry* with $z_s = \frac{8}{9}\sqrt{6}$. The reason for choosing the *near SU(6) symmetry* parametrization is because we have checked that SU(6) fixes $z_s = \sqrt{6}$, which results in a very repulsive Ξ potential $U_\Xi = +60$ MeV, in disagreement with expected values running from -40 to 40 MeV [19]. Then only α_s remains to be fixed. Now we attach α_s to α_v forcing the U_Λ potential to be equal to -28 MeV [22]. This leaves our theory completely in tune with the SU(3) symmetry group for all hyperon-mesons couplings, and only one free parameter is left to be varied, α_v.

[1] P. B. Demorest *et al.*, Nature **467**, 1081 (2010).
[2] J. Antoniadis *et al.*, Science **340**, 1233232 (2013).
[3] N. K. Glendenning, *Compact Stars*, 2nd ed. (Springer, New York, 2000).
[4] H. J. Schulze and T. Rijken, Phys. Rev. C **84**, 035801 (2011).
[5] M. Baldo, G. F. Burgio, and H. J. Schulze, Phys. Rev. C **58**, 3688 (1998).
[6] M. Baldo, G. F. Burgio, and H. J. Schulze, Phys. Rev. C **61**, 055801 (2000).
[7] H. Đapo, B.-J. Schaefer, and J. Wambach, Phys. Rev. C **81**, 035803 (2010).
[8] S. Balberg, I. Lichtenstadt, and G. Cook, Astrophys. J. Suppl. **121**, 515 (1999).
[9] B. D. Serot, Rep. Prog. Phys. **55**, 1855 (1992).
[10] P. Haensel, A. Y. Potekhin, and D. G. Yakovlev, *Neutron Stars, Equation of State and Structure* (Springer, New York, 2006).
[11] F. Hofmann, C. M. Keil, and H. Lenske, Phys. Rev. C **64**, 025804 (2001).
[12] A. M. S. Santos and D. P. Menezes, Phys. Rev. C **69**, 045803 (2004).
[13] N. Glendenning, Nucl. Phys. A **505**, 779 (1989).
[14] M. Paoli and D. P. Menezes, Eur. J. Phys. A **46**, 413 (2010).
[15] T. Katayama, T. Miyatsu, and K. Saito, Astrophys. J. Suppl. **203**, 22 (2012).
[16] R. Cavagnoli, D. P. Menezes, and C. Providencia, Phys. Rev. C **84**, 065810 (2011).
[17] J. Ellis, J. I. Kapusta, and K. A. Olive, Nucl. Phys. B **348**, 345 (1991).
[18] J. Schaffner and I. N. Mishustin, Phys. Rev. C **53**, 1416 (1996).
[19] S. Weissenborn, D. Chatterjee, and J. Schaffner-Bielich, Nucl. Phys. A **881**, 62 (2012).
[20] S. Weissenborn, D. Chatterjee, and J. Schaffner-Bielich, Phys. Rev. C **85**, 065802 (2012).
[21] A. Pais, Rev. Mod. Phys. **38**, 215 (1966).
[22] N. K. Glendenning, S. A. Moszkowski, Phys. Rev. Lett. **67**, 2414 (1991).
[23] J. Schaffner *et al.*, Ann. Phys. **235**, 35 (1994); A. Taurines *et al.*, Mod. Phys. Lett. A **15**, 1789 (2000).
[24] C. Dover and A. Gal, Prog. Part. Nucl. Phys. **12**, 171 (1984).
[25] J. Schaffner-Bielich and A. Gal, Phys. Rev. C **62**, 034311 (2000).
[26] Zhao, Xian-Feng, Chin. Astron. Astrophys. **35**, 285 (2011).
[27] M. Rufa *et al.*, J. Phys. G **13**, L143 (1987).
[28] L. L. Lopes and D. P. Menezes, Braz. J. Phys. **42**, 428 (2012).
[29] T. Miyatsu, M. K. Cheoun, and K. Saito, Phys. Rev. C **88**, 015802 (2013).
[30] I. Sagert, L. Tolos, D. Chatterjee, J. Schaffner-Bielich, and C. Sturm, Phys. Rev. C **86**, 045802 (2012).
[31] P. Danielewicz *et al.*, Science **298**, 1592 (2002).
[32] G. A. Lalazissis, J. Konig, and P. Ring, Phys. Rev. C **55**, 540 (1997).
[33] A. Steiner, M. Prakash, and J. Lattimer, Phys. Lett. B **486**, 239 (2000).
[34] J. Boguta and A. R. Bodmer, Nucl. Phys. A **292**, 413 (1977).
[35] M. M. Nagels, T. A. Rijken, and J. J. de Swart, Phys. Rev. D **20**, 1633 (1979).
[36] W. Greiner and B. Muller, *Quantum Mechanics, Symmetries*, 2nd ed. (Springer, New York, 1994).
[37] Th. A. Rijken, V. G. J. Stoks, and Y. Yamamoto, Phys. Rev. C **59**, 21 (1999).
[38] W. Greiner, L. Neise, and H. Stocker, *Thermodynamics and Statistical Mechanics* (Springer, New York, 1995).
[39] S. Pal, M. Hanauske, I. Zakout, H. Stocker, and W. Greiner, Phys. Rev. C **60**, 015802 (1999).
[40] R. Cavagnoli and D. P. Menezes, J. Phys. G **35**, 115202 (2008).
[41] J. J. Sakurai, Ann. Phys. **11**, 1 (1960).
[42] S. J. Dong, J. F. Lagae, and K. F. Liu, Phys. Rev. D **54**, 5496 (1996).
[43] P. Ellis, R. Knorren, and M. Prakash, Phys. Lett. B **349**, 11 (1995).
[44] M. Engelhardt, Phys. Rev. D **86**, 114510 (2012).
[45] P. M. Hohler and M. A. Stephanov, Phys. Rev. D **80**, 066002 (2009).
[46] J. Noronha-Hostler, J. Noronha, and C. Greiner, Phys. Rev. Lett. **103**, 172302 (2009).
[47] N. Chamel *et al.*, Astron. Astrophys. **553**, A22 (2013).
[48] T. Renk, Eur. Phys. J. C **49**, 13 (2007).
[49] R. B. Neufeld and T. Renk, Phys. Rev. C **82**, 044903 (2010).
[50] M. B. Tsang *et al.*, Phys. Rev. C **86**, 015803 (2012).
[51] P. B. Muzinger and J. Stachel, Ann. Rev. Nucl. Part. Sci. **37**, 97 (1987).

[52] J. Cottam, F. Paerels, and M. Mendez, Nature **420**, 51 (2002).
[53] D. Sanwal *et al*., Astrophys. J. Lett. **574**, 61 (2002).
[54] R. Romani *et al*., Astrophys. J. Lett. **760**, L36 (2012).
[55] J. R. Oppenheimer and G. M. Volkoff, Phys. Rev. **55**, 374 (1939).
[56] G. Baym, C. Pethick, and P. Sutherland, Astrophys. J. **170**, 299 (1971).
[57] K. Hebeler, J. M. Lattimer, C. J. Pethick, and A. Schwenk, Phys. Rev. Lett. **105**, 161102 (2010).
[58] S. Gandolfi, J. Carlson, and S. Reddy, Phys. Rev. C **85**, 032801(R) (2012).
[59] Constança Providência *et al*., Eur. Phys. J. A (2014) arXiv:1307.1436 [nucl-th].
[60] A. W. Steiner and S. Gandolfi, Phys. Rev. Lett **108**, 081102 (2012).
[61] J. M. Lattimer and Y. Lim, Astrophys. J. **771**, 51 (2013).
[62] A. W. Steiner, J. M. Lattimer, and E. Brown, Astropys. J. **722**, 33 (2010).
[63] S. Guillot, M. Servillat, N. A. Webb, and R. E. Rutledge, arXiv:1302.0023v2 [astro-ph.HE].
[64] J. M. Lattimer and A. W. Steiner, arXiv:1305.3242 [astro-ph.HE].
[65] B. G. Todd-Rutel and J. Piekarewicz, Phys. Rev. Lett. **95**, 122501 (2005).
[66] F. J. Fattoyev, C. J. Horowitz, J. Piekarewicz, and G. Shen, Phys. Rev. C **82**, 055803 (2010).
[67] G. Shen, C. J. Horowitz, and E. O'Connor, Phys. Rev. C **83**, 065808 (2011).
[68] Wynn C. G. Ho *et al*., Mon. Not. R. Astron. Soc. **375**, 821 (2007).
[69] Lie-Wen Chen, Che Ming Ko, and Bao-An Li, Phys. Rev. C **72**, 064309 (2005).
[70] C. E. Rhoades and R. Ruffini, Phys. Rev. Lett. **32**, 324 (1974).
[71] M. E. Gusakov and P. Haensel, Mon. Not. Royal Astr. Soc. (to be published).
[72] V. Dexheimer, R. Negreiros, and S. Schramm, Eur. Phys. J. A **48**, 189 (2012); V. Dexheimer, D. P. Menezes, and M. Strickland, J. Phys. G: Nucl. Part. Phys. **41**, 015203 (2014).
[73] R. Casali, L. B. Castro, and D. P. Menezes (2014) arXiv:1307.2651 [astro-ph.SR].
[74] M. Nagels, T. Rijken, and J. J. Swart, Ann. Phys. **79**, 338 (1973).
[75] J. J. Swart, Rev. Mod. Phys. **35**, 916 (1963); **37**, 326(E) (1965).
[76] Fl. Stancu, *Group Theory in Subnuclear Physics* (Clarendon Press, Oxford, 1996).
[77] P. McNamee and F. Chilton, Rev. Mod. Phys. **36**, 1005 (1964).
[78] M. Nagels, T. Rijken, and J. J. Swart, Phys. Rev. D **12**, 744 (1975).
[79] M. Nagels, T. Rijken, and J. J. Swart, Phys. Rev. D **15**, 2547 (1977).
[80] P. Carruthers, Phys. Rev. D **3**, 959 (1971).